Capillary Fracturing in Granular Media

Ran Holtzman,[1,2] Michael L. Szulczewski,[1] and Ruben Juanes[1,*]

[1]*Massachusetts Institute of Technology, 77 Massachusetts Avenue, Building 48, Cambridge, Massachusetts 02139, USA*
[2]*The Hebrew University of Jerusalem, P.O. Box 12, Rehovot 76100, Israel*

(Received 25 February 2012; published 28 June 2012)

We study the displacement of immiscible fluids in deformable, noncohesive granular media. Experimentally, we inject air into a thin bed of water-saturated glass beads and observe the invasion morphology. The control parameters are the injection rate, the bead size, and the confining stress. We identify three invasion regimes: capillary fingering, viscous fingering, and ''capillary fracturing,'' where capillary forces overcome frictional resistance and induce the opening of conduits. We derive two dimensionless numbers that govern the transition among the different regimes: a modified capillary number and a fracturing number. The experiments and analysis predict the emergence of fracturing in fine-grained media under low confining stress, a phenomenon that likely plays a fundamental role in many natural processes such as primary oil migration, methane venting from lake sediments, and the formation of desiccation cracks.

DOI: 10.1103/PhysRevLett.108.264504 PACS numbers: 47.56.+r, 47.20.−k, 47.54.−r

The invasion of one fluid into a porous medium filled with another fluid occurs in many natural and industrial processes. These processes include gas venting, hydrocarbon recovery, geologic CO_2 sequestration, and soil wetting and drying. Pore-scale disorder, hydrodynamic instabilities, and mechanical deformation of the pore geometry result in complex displacement patterns. Understanding the emergent patterns is both scientifically fascinating and technologically important [1].

Fluid-fluid displacements in rigid porous media have been studied in depth. While fundamental questions remain, previous studies have provided a basic understanding of the different displacement regimes, including compact displacement, capillary fingering, and viscous fingering, through laboratory experiments and computer simulations [2–11]. These regimes depend on the flow velocity, the degree of pore-scale disorder, and the interfacial tension and viscosity contrast between the fluids.

In a deformable medium such as a granular bed, fluid flow can displace the particles and affect the pore geometry, which in turn can affect the flow. This interplay between the displacements of the fluids and the particles leads to a variety of patterns, including desiccation cracks [12], granular fingers [13], labyrinth structures [14], stick-slip bubbles [15], open channels [16,17], and fractures [15,18–22].

While fracturing during gas invasion in liquid-saturated media has been observed in several experiments [15,18–22] and simulations [23], the underlying mechanisms and controlling parameters behind the morphodynamics of gas invasion in liquid-filled deformable granular media remain poorly understood. Holtzman and Juanes [24] developed a model that predicts the transitions among capillary fingering, viscous fingering, and fracturing. The authors used pore-scale simulations and scaling analysis to show that fracturing caused by elastic deformation of particles is the dominant mode of invasion for fine, soft particles under low confining stress. In this Letter, we study fracturing in a system of rigid particles. We show that frictional sliding, rather than elastic deformation, is the key mechanism controlling fracturing. We provide experimental evidence for three displacement regimes—capillary fingering, viscous fingering, and capillary fracturing—and derive two dimensionless groups that govern the transitions among these regimes.

We inject air into a thin bed of water-saturated glass beads packed in a cylindrical cell. We prepare each granular bed by pouring beads into the cell and then vibrating it to increase the packing homogeneity [25]. There are three control parameters: the mean particle diameter, d, the air injection rate, q, and the confining weight, w. The confinement is applied by weights placed on a rigid disk that rests on top of the beads. To allow fluids (but not the particles) to leave the cell, the disk is made slightly smaller than the interior of the cell (inner diameter L), leading to a thin gap along the edge of the cell. We inject the fluids with a syringe pump at a fixed rate to the center of the cell, and image the invasion pattern during the experiment with a digital camera (Fig. 1). To analyze the images, we subtract the initial image prior to injection. For most experimental conditions, we perform repeatability experiments.

The experiments exhibit three displacement regimes: viscous fingering, capillary fingering, and capillary fracturing. We identify the regimes based on the qualitative characteristics of the invasion pattern, as has been done previously [2,4,7,18,24]. In viscous fingering, the air-water interface grows continuously and at several locations simultaneously. The resulting pattern is radial and exhibits thin fingers and few trapped water clusters. The pattern appears more space-filling than in two-dimensional experiments

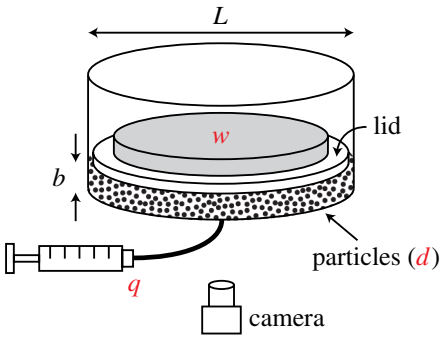

FIG. 1 (color online). Experimental setup: a thin bed (thickness b) of water-saturated glass beads (mean diameter d) is confined in a cylindrical acrylic cell (internal diameter L). Vertical confinement is supplied by a weight, w, placed on a disk ("lid") that rests on top of the beads. The disk is slightly smaller than the cell to allow fluids (but not particles) to leave the cell. Air is injected into the center of the cell at a fixed flow rate q. Time-lapse images are captured by a camera placed underneath the cell.

(e.g. in a monolayer of beads [5]) because in three dimensions water clusters that appear to be trapped actually remain connected vertically across layers (Fig. 2(a); Video 1 in the Supplemental Material [25]). In capillary fingering, the air-water interface propagates intermittently (Fig. 2(b); Video 2 [25]). Since the air invasion is controlled by the spatial distribution of capillary entry pressures, which in turn is controlled by the distribution of pore throat sizes, the patterns are typically not radially symmetric, as has been previously observed [26,27]. In capillary fracturing, the air-water interface advances continuously in thin fingers with long, straight segments. The resulting pattern is asymmetric and occupies a much smaller portion of the cell compared with capillary fingering and viscous fingering. While capillary fracturing exhibits a distinct morphology, we identify it exclusively from visual observation of bead displacements. These displacements appear as "halos" in the subtracted images, caused by changes to light reflection

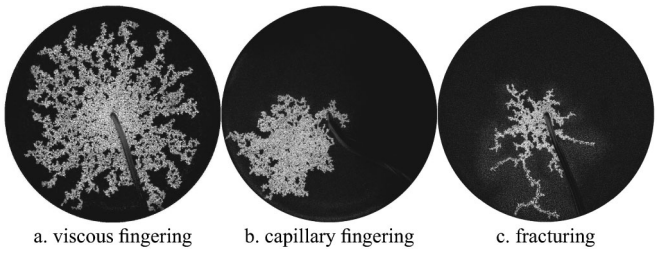

FIG. 2. Examples of experimentally observed patterns. We classify these patterns into three regimes: viscous fingering, capillary fingering, and fracturing. In these difference images, obtained by subtracting the initial image prior to air invasion, air shows as clear white, water and undisturbed beads as black, and deformed regions as a sparkly halo (bead displacements change the reflected light). Experimental conditions: $d = 360$ μm; $w = 181$ N (a),(b) and 3 N (c); and $q = 100$ (a), 0.1 (b), and 1 mL/min (c).

by bead displacements (Fig. 2(c); Video 3 in the Supplemental Material [25]). The three regimes display transition zones, in which the invasion patterns exhibit mixed characteristics of the end-member patterns.

The mode of displacement depends on the competition between forces. The transition between capillary fingering and viscous fingering depends on the competition between viscous forces and capillary forces [8,10], whereas the transition between fingering and fracturing depends on the competition between hydrodynamic forces that promote pore opening, and mechanical forces that resist it. Since these forces depend on a combination of the control parameters, the same transition between the regimes can be achieved by changing different parameters: the displacement can transition from capillary fingering to viscous fingering by increasing the injection rate, q, or reducing the bead size, d; and from fingering to fracturing by reducing the confining weight, w, or the bead size, d (Fig. 3). The wide transition zone between capillary and viscous fingering has been observed previously [2], and is due to gradual changes in the governing forces with the experimental conditions. The capillary fracturing patterns transition from few, small fractures to many, large fractures as the confinement is reduced, though this trend is not conveyed in the plots since our identification of fracturing does not account for the frequency or magnitude of bead displacements. Repetition of experiments with similar conditions yields the same invasion regime, even if the details of the invasion pattern differ.

We rationalize these transitions by computing the ratio between the driving forces that promote the development of a particular pattern. For a rigid medium, the transition between capillary fingering and viscous fingering occurs when the characteristic macroscopic viscous pressure drop in the direction parallel to flow, δp_v, exceeds the variation in capillary entry pressures along the interface, δp_c. We compute δp_v as $\nabla p_v L$, and use Darcy's law, $\nabla p_v \sim \eta v/k$ with $k \sim d^2$, to obtain $\delta p_v \sim \eta v L/d^2$. Here, η is the dynamic viscosity of water, and $v \sim q/(bd)$ is the flow velocity. We use a fixed value of the macroscopic length scale with $L \gg d$ for the viscous pressure drop in the defending phase, an assumption that is justified during the initial stages of the invasion but that becomes questionable at later stages, when the invasion front approaches the system's boundaries and becomes fractal [28]. The maximum difference in capillary pressures along the interface is $\delta p_c = \gamma/r_{\min} - \gamma/r_{\max} \sim \gamma\chi(\lambda)/\bar{r}$, where γ is the air-water interfacial tension, $\bar{r} \sim d$ is the mean throat aperture, and $\chi(\lambda)$ describes the distribution of capillary entry pressures, a function of the degree of pore-scale disorder $\lambda \in (0, 1)$ [24]. For instance, for a uniform aperture distribution, $r \in [1 - \lambda, 1 + \lambda]\bar{r}$, we get $\chi(\lambda) = \lambda/(1 - \lambda^2)$.

The transition from viscous to capillary fingering occurs when $\delta p_v \sim \delta p_c$, and is therefore controlled by the following "modified capillary number," $\mathrm{Ca}^* = \delta p_v/\delta p_c$:

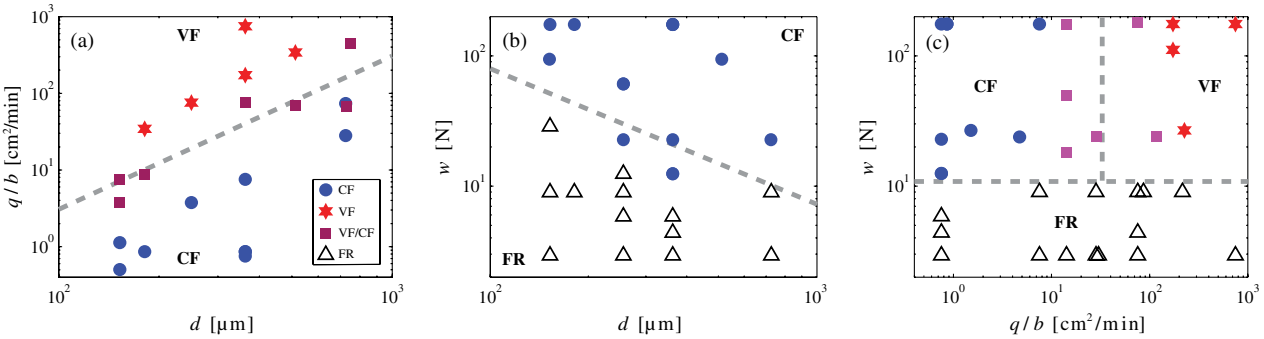

FIG. 3 (color online). Phase diagrams of fluid-fluid displacement patterns in the experiments. The diagrams demonstrate how changing the control parameters affects the patterns. Diagram (a) shows that the transition from viscous fingering (VF) to capillary fingering (CF) occurs at $q/b \sim d^2$ (fixing $w = 181$ N). Intermediate patterns are marked as VF/CF. Diagram (b) shows that the transition from capillary fingering to fracturing (FR) occurs at $w \sim d^{-1}$ ($q = 0.1$ mL/min). Diagram (c) shows that the transition from fingering to fracturing is independent of q/b ($d = 360$ μm).

$$\mathrm{Ca}^* = \mathrm{Ca}\frac{L}{d}\chi^{-1}(\lambda) = \frac{\eta q L}{\gamma b d^2}\chi^{-1}(\lambda), \tag{1}$$

where $\mathrm{Ca} = \eta v/\gamma$ is the classical capillary number [2]. For a given pair of fluids, the viscosity and interfacial tension are fixed. Assuming similar disorder across experiments, this scaling suggests that the phase boundary between viscous fingering and capillary fingering is $q/b \sim d^2$, in agreement with our experimental data [Fig. 3(a)].

In a granular medium, fractures open when forces exerted by the fluids exceed the mechanical forces that resist particle rearrangements. In cohesionless granular material, these forces include elastic compression and friction. For systems with densely packed, highly compliant particles, pore opening occurs by means of particle deformation [24]. However, for many types of particles including most mineral grains and manufactured beads, the high particle stiffness limits interparticle deformation, making frictional sliding the dominant deformation mechanism that alters the pore geometry.

To demonstrate this quantitatively, we compare the two characteristic resisting forces. The increment in elastic compressive force associated with a relative particle displacement (interparticle deformation) Δh is $\Delta f_e \sim K\Delta h$, where K is the interparticle contact stiffness. The stiffness $K \sim E\sqrt{dh}$ is computed by assuming Hertzian interparticle forces, $f_e \sim E\sqrt{d}h^{3/2}$, where E is the Young's modulus of the particle material and h is the total interparticle deformation [29]. We evaluate K at $h = h_0$, where h_0 is the initial (prior to fracturing) interparticle deformation. We obtain h_0 from the expression for the initial interparticle force, $f_{e,0} \sim E\sqrt{d}h_0^{3/2}$, which, assuming homogenous force distribution, can also be evaluated from the vertical confinement, $f_{e,0} \sim w/(L/d)^2$. Fracturing requires a sufficiently large change in the throat apertures, $\lambda\bar{r} \sim \lambda d$, implying interparticle displacement of $\Delta h \sim \lambda d$. The elastic resisting force is therefore $\Delta f_e = \lambda E^{2/3}L^{-2/3}w^{1/3}d^2$. We compare this force with the frictional resistance force, evaluated from the limiting value at sliding, $\Delta f_f \sim \mu f_{e,0} \sim \mu w/(L/d)^2$, where μ is the coefficient of friction. The resulting force ratio is then

$$\frac{\Delta f_e}{\Delta f_f} = \frac{\lambda E^{2/3}L^{4/3}}{\mu w^{2/3}}. \tag{2}$$

For our experimental system, with $E = 70$ GPa, $\mu = 0.3$ [30], $L = 0.2$ m, $\lambda = 0.75$, and $w = 3$–181 N, the elastic resistance is 5–6 orders of magnitude higher than frictional resistance, suggesting that pore opening occurs by overcoming friction. Elasticity would play an important role in fracturing only for much softer beads and much larger confining stresses.

We predict the emergence of fracturing through a dimensionless parameter we call the "fracturing number," N_f, that measures the system deformability as the ratio of the pressure force that drives fracturing, Δf_p, and the resisting force, Δf_f. The driving force is the product of the local pressure difference at the front tip, Δp, and the area over which it acts, $A_p \sim d^2$. The pressure difference is the sum of the capillary pressure, γ/d, and the local viscous pressure drop, $\nabla p_v d \sim \eta v/d$. Thus, $\Delta f_p = \gamma d + \eta v d = \gamma d(1 + \mathrm{Ca})$, and

$$N_f = \frac{\gamma L^2}{\mu w d}(1 + \mathrm{Ca}). \tag{3}$$

This scaling suggests that, for a given fluid pair, particle material, and system size, the transition from fingering to fracturing occurs at $w \sim d^{-1}$. This is consistent with our observations [Fig. 3(b)]. While the scaling accounts for the effects of both the capillary pressure and the local viscous pressure drop, the capillary pressure is the dominant cause of fracturing in our experiments (with $\eta \approx 10^{-3}$ Pa s, $\gamma \approx 0.07$ N/m, $q \leq 100$ mL/min, and therefore $\mathrm{Ca} \ll 1$). As a result, the observed transition does not depend on the flow rate [Fig. 3(c)].

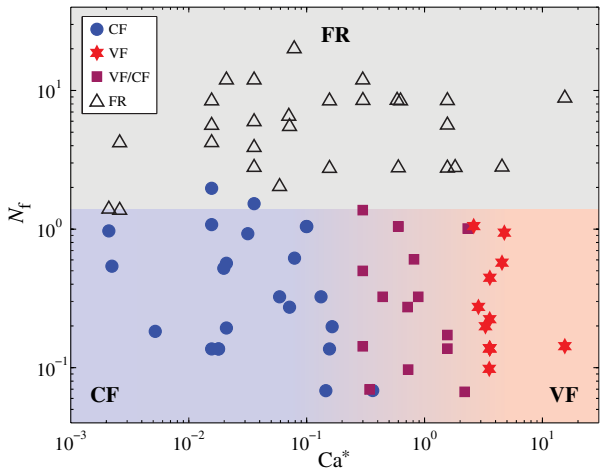

FIG. 4 (color online). Phase diagram of drainage in granular media, showing three invasion regimes: viscous fingering (VF), capillary fingering (CF), and fracturing (FR). The tendency to fracture is characterized by the "fracturing number" N_f: drainage is dominated by fracturing in systems with $N_f \gg 1$. At lower N_f values, the type of fingering depends on the modified capillary number, Ca*.

The scaling analyses allow us to collapse our data from a three-parameter dimensional phase space (q, w, d) into a two-parameter dimensionless space (Ca*, N_f). For $N_f \gg 1$, fracturing is the dominant mode of invasion. For $N_f \ll 1$, the medium is essentially rigid (negligible particle rearrangements), and the transition from capillary to viscous fingering occurs at Ca* ≈ 1 (Fig. 4).

These results demonstrate and rationalize the crossover among three regimes of drainage in granular media: capillary fingering, viscous fingering, and capillary fracturing. They show that the crossover between capillary fingering and viscous fingering can be characterized by a modified capillary number, Ca*. Our results demonstrate the emergence of capillary fracturing, in which capillary forces dilate pore throats by exceeding the internal frictional resistance of the medium. The scaling of the fracturing number [Eq. (3)] suggests that, in granular systems with rigid solid particles, capillary fracturing tends to occur when the particle size falls below a critical value, $d_c \sim \gamma L^2/\mu w$. This provides a rationale to observations of capillary-induced fracturing in a variety of natural systems, such as drying in granular media [12,20], gas venting in lake sediments [19,31], and hydrate veins in the ocean floor [32]. In all of these settings, the formation of fractures provides open conduits that allow fast exchange of elements, which are likely critical to the water, carbon, and energy budgets in the biosphere.

We thank J. Darby and R. Martinez for their contributions to the experiments. We gratefully acknowledge financial support for this work, provided by Eni S.p.A. and by the ARCO Chair in Energy Studies.

*juanes@mit.edu

[1] M. Sahimi, *Flow and Transport in Porous Media and Fractured Rock* (VCH, New York, 2011), 2nd ed.
[2] R. Lenormand, E. Touboul, and C. Zarcone, J. Fluid Mech. **189**, 165 (1988).
[3] D. Wilkinson and J. Willemsen, J. Phys. A **16**, 3365 (1983).
[4] L. Paterson, Phys. Rev. Lett. **52**, 1621 (1984).
[5] K. J. Måløy, J. Feder, and T. Jøssang, Phys. Rev. Lett. **55**, 2688 (1985).
[6] J. P. Stokes, D. A. Weitz, J. P. Gollub, A. Dougherty, M. O. Robbins, P. M. Chaikin, and H. M. Lindsay, Phys. Rev. Lett. **57**, 1718 (1986).
[7] J.-D. Chen and D. Wilkinson, Phys. Rev. Lett. **55**, 1892 (1985).
[8] J. F. Fernández, R. Rangel, and J. Rivero, Phys. Rev. Lett. **67**, 2958 (1991).
[9] Y. C. Yortsos, B. Xu, and D. Salin, Phys. Rev. Lett. **79**, 4581 (1997).
[10] M. Ferer, C. Ji, G. S. Bromhal, J. Cook, G. Ahmadi, and D. H. Smith, Phys. Rev. E **70**, 016303 (2004).
[11] R. Toussaint, G. Løvoll, Y. Méheust, K. J. Måløy, and J. Schmittbuhl, Europhys. Lett. **71**, 583 (2005).
[12] P. Meakin, Science **252**, 226 (1991).
[13] X. Cheng, L. Xu, A. Patterson, H. M. Jaeger, and S. R. Nagel, Nature Phys. **4**, 234 (2008).
[14] B. Sandnes, H. A. Knudsen, K. J. Måløy, and E. G. Flekkøy, Phys. Rev. Lett. **99**, 038001 (2007).
[15] B. Sandnes, E. Flekkøy, H. Knudsen, K. J. Måløy, and H. See, Nature Commun. **2**, 288 (2011).
[16] X.-Z. Kong, W. Kinzelbach, and F. Stauffer, Chem. Eng. Sci. **65**, 4652 (2010).
[17] G. Varas, V. Vidal, and J.-C. Géminard, Phys. Rev. E **83**, 061302 (2011).
[18] C. Chevalier, A. Lindner, M. Leroux, and E. Clement, J. Non-Newtonian Fluid Mech. **158**, 63 (2009).
[19] B. P. Boudreau, C. Algar, B. D. Johnson, I. Croudace, A. Reed, Y. Furukawa, K. M. Dorgan, P. A. Jumars, A. S. Grader, and B. S. Gardiner, Geology **33**, 517 (2005).
[20] L. Xu, S. Davies, A. B. Schofield, and D. A. Weitz, Phys. Rev. Lett. **101**, 094502 (2008).
[21] H. Shin and J. C. Santamarina, Earth Planet. Sci. Lett. **299**, 180 (2010).
[22] J.-H. Choi, Y. Seol, R. Boswell, and R. Juanes, Geophys. Res. Lett. **38**, L17310 (2011).
[23] A. K. Jain and R. Juanes, J. Geophys. Res. **114**, B08101 (2009).
[24] R. Holtzman and R. Juanes, Phys. Rev. E **82**, 046305 (2010).
[25] See Supplemental Material at http://link.aps.org/supplemental/10.1103/PhysRevLett.108.264504 for details of the experimental procedure and data analysis, and movies showing the development of the displacement patterns.
[26] R. Lenormand, Physica A (Amsterdam) **140**, 114 (1986).
[27] V. Frette, J. Feder, T. Jøssang, P. Meakin, and K. J. Måløy, Phys. Rev. E **50**, 2881 (1994).
[28] R. Lenormand, Proc. R. Soc. A **423**, 159 (1989).
[29] K. L. Johnson, *Contact Mechanics* (Cambridge University Press, Cambridge, England, 1987).
[30] Y. Li, Y. Xu, and C. Thornton, Powder Technol. **160**, 219 (2005).
[31] B. P. Scandella, C. Varadharajan, H. Hemond, C. Ruppel, and R. Juanes, Geophys. Res. Lett. **38**, L06408 (2011).
[32] K. C. Hester and P. G. Brewer, Annu. Rev. Mar. Sci. **1**, 303 (2009).